



The importance of being a cube: Active cubes in a microchannel

Martin Kaiser^{a,*}, Sofia S. Kantorovich^{c,b}

^a University of Vienna, Physics Faculty/Research Platform MMM Mathematics-Magnetism-Materials, Vienna, Austria

^b Faculty of Physics, University of Vienna, Boltzmannngasse 5, 1090 Vienna, Austria

^c Ural Federal University, Lenin Av. 51, Vienna, Austria



ARTICLE INFO

Article history:

Received 10 February 2022

Revised 28 April 2022

Accepted 30 April 2022

Available online 10 May 2022

Keywords:

Active Matter

Active Cube

Hydrodynamics

Microchannel

ABSTRACT

Cubic shaped micrometer and nanometer sized colloids have become a popular research subject in experimental and theoretical soft matter physics. However, they are underrepresented in the field of active matter where the most investigated colloidal shapes are spheres or rods, for which hydrodynamic interactions vary from cube ones due to distinct body shape anisotropies. In this article, we are building on this knowledge by performing simulations to elucidate how active cubes in microchannels interact hydrodynamically with planar and curved boundaries through the flow field generated by an active force. We find that cubes tend to not show the same oscillatory behaviour previously found for other particle shapes, but move along a straight line near the channel centre for a range of initial conditions and parameters that can be accounted for in simulations. This effect arises through the cubes unique shape anisotropy interacting with the flow field and demonstrates that a cube constitutes an interesting hydrodynamic shape that deserves more attention in colloidal active matter research, in order to fully utilise its potential as an enrichment to commonly used particle shapes.

© 2022 The Authors. Published by Elsevier B.V. This is an open access article under the CC BY license (<http://creativecommons.org/licenses/by/4.0/>).

1. Introduction

The idea of creating and using micron sized motors has become more and more popular over the past years due to advances in fabrication and measuring techniques. The interdisciplinary research done in this field promises novel concepts to utilise suitable motors for mechanical and biological applications. The key factors that make a micromotor suitable are its ability to propel itself, while at the same time having a predictable trajectory and diffusive behaviour. There are a multitude of experimental and theoretical works that focus on the characterisation and explanation of emerging behaviour in active matter systems (e.g. collective swarming), propulsion mechanisms and interaction with geometrical constraints [1–6]. The latter is a key feature of micron sized active systems that make them fundamentally different than passively diffusing particles. Especially in colloidal systems, there exists a selection of computational modelling techniques that allow for a detailed investigation of colloid/boundary interactions and their influence on the colloid trajectory [7–9]. These models have repeatedly shown that active colloids like to accumulate near boundaries, even if no other attractive force between the particle and boundary is present. This has also been shown in experiments,

where boundaries are usually realised as flat walls or walls with edges [10–13].

The dynamics at obstacles is determined by an additional boundary induced velocity and torque through different mechanisms that depend on the particle shape and fluid properties. Included in those mechanisms are hydrodynamic, chemical and steric interactions [14]. For single spheres at a flat wall, these interactions, combined with the relative strength of the activity with respect to thermal fluctuations, typically lead to a characteristic time that the particle spends at the boundary before it is reoriented and escaping away from it [15,16]. In the absence of thermal noise, stable swimming along the boundary or trapping can occur [17–19]. In systems of spherical active particle ensembles, these interactions lead to a collective accumulation near the boundary. [20] have furthermore found that squirmers can experience an oscillatory motion as a result of competing forces that emerge from hydrodynamic and repulsive particle/wall interactions.

Recently, [21] have shown that active rods and cylinders in micro channels consisting of two planar walls, are moving in an oscillatory motion around the channels centre, far away from the boundaries [21]. They attribute this behaviour to the higher moments of the flow field generated by the swimmer, considering a point force/counter-force formalism for active swimming. While for pusher type particles (particles with an extensile flow with out-

* Corresponding author.

E-mail address: martin.kaiser@univie.ac.at (M. Kaiser).

wards pointing forces), the hydrodynamic moments force the particle closer to the wall, for puller type particles (contractile flow field with the point forces pointing towards each other) the opposite is the case and the particles end up in the centre of the channel undergoing a damped oscillation. Due to the orientation of force/counter-force, pushers and pullers created the inverse flow field of each other.

While cubes are by now well established in soft matter and microfluidics research, using them as active agents is not yet a common practice [22–24], although they offer a great variety of observed habits due to their shape. For example, magnetic cubes on the micro and nanoscale are reportedly different in their assembly behaviour due to the richer possibilities of magnetisation orientation compared to isotropic spheres [25–27]. Furthermore, we have shown in past research that the diffusion of active, magnetic, nanometer sized colloids can be easily controlled by weak magnetic fields in isolated and bulk particle systems [28,29]. From a hydrodynamics point of view, cubes offer a type of anisotropy that is hard to find in other particle shapes. [30] conducted high resolution simulations of a cube in a uniform low Reynolds number translational flow and simulations of a rotating cube in a quiescent fluid. Measuring the forces and torques acting on the cube, they found that its translational and rotational motion at low Reynolds numbers are decoupled, meaning that a rotation of the cube does not induce lateral motion and vice versa. Additionally, the friction tensor is diagonal (therefore symmetric), where the diagonal entries can be estimated as,

$$\gamma_{cube}^T = 1.384 \cdot (3\pi\eta d), \quad (1)$$

$$\gamma_{cube}^R = 2.552 \cdot (\pi\eta d^3), \quad (2)$$

for rotation and translation respectively. This means that the friction for a cube can be treated like that of a sphere, for which the numerical prefactors of both frictions is 1, if the Reynolds number is sufficiently lower than unity. This is not the case, for example, for rods and cylinders, where the entries in the friction tensor are not equal and can therefore not be treated in the same fashion [31,32].

For active colloidal systems, the complex flow fields produced by the propulsion mechanisms and their interaction with the colloid are the defining factor for the colloids trajectory in confinement. The above mentioned frictional behaviour of a cube therefore suggests to investigate differences in cubic shaped colloids in settings where the behaviour of differently shaped particles is known. In this article, we set out to investigate the behaviour of isolated, micro meter sized cubic active colloids in a micron sized channel, similarly to the previous work of [21], characterising their trajectories and getting a detailed look at the reorientation mechanisms that the cubes experience.

2. Methods

To model the motion of an active cube in a micron sized channel, we employ a Lattice Boltzmann (LB) hydrodynamics solver that is coupled to the Molecular Dynamics (MD) program package *ESPResSo*(v4.1.4) [33,34]. The LB method is a continuum and lattice based procedure that attains fluid velocity fields by propagating probability densities on the individual nodes of the space discretising lattice, which makes it per construction well parallelisable and efficient on modern computing hardware. The LB solver is integrated to exchange forces with classic MD particles via the coupling scheme proposed by [35,35], which states the force exerted on a point-particle by the surrounding fluid as,

$$\vec{F} = -\gamma_{LB}(\vec{u}_{part} - \vec{u}_{fluid}). \quad (3)$$

Here, \vec{u}_{fluid} and \vec{u}_{part} are the velocities of the fluid and the particle, γ_{LB} is the LB friction parameter that tunes the interaction between particles and the fluid.

ESPResSo utilises reduced simulation units (SU) to characterise the system. For this, we have to define a length, mass, energy and timescale that in return define every other quantity in our simulation. The most important simulation parameters, as well as their SI counterpart can be found in Table 1. An important note has to be made regarding the solvent viscosity, which is chosen to be a tenth of the viscosity of water at 298 K (25C°). This is done for a technical reason, since using the original viscosity would lead to problematic simulation parameters that would not allow for the accumulation of the data in a reasonable time frame. Our choice of viscosity allows not only for reasonable parameters that maintain the hydrodynamic interactions, but for a greatly decreased computation time.

The aim of this article is not to model an experimental system from a specific reference, but rather to stay within physical parameters by using a generic $5\mu\text{m}$ hollow silica cube with a shell thickness of $1\mu\text{m}$ as reference to derive the simulation parameters. The assumed colloid has a shape parameter $q = 2.3$, that defines the cubicity of the particle with side length a via the superball equation,

$$\left(\frac{x}{a}\right)^{2q} + \left(\frac{y}{a}\right)^{2q} + \left(\frac{z}{a}\right)^{2q} = 1. \quad (4)$$

Rather than opting for the representation of a perfect cube, which is not realisable experimentally, we chose the given shape, keeping in mind existing superball colloids of different material [36,37]. The approach used in simulations to resolve the shape of the colloid is the so called "raspberry model". The raspberry model was invented to circumvent the inability of the LB method to apply torques on point MD particles, by discretising the body of essentially any shape by spherical MD building blocks. The idea is that the discretising MD blocks are rigidly attached, thus transferring any forces applied by the fluid, to a central particle which carries all the information about the colloid (e.g. mass, moments of inertia). Typically, as it is also the case for our simulations, the choice of a Lattice Boltzmann grid spacing $a_{grid} = 1[\text{SU}]$ leads to a hydrodynamic radius of a single discretisation point, therefore also to a hydrodynamic radius of the colloid, matching the extent of the steric shell of the modelled colloid. The steric diameter σ of one discretisation point in simulations is chosen to be unity. The cube consists of 64 coupling points on a regular grid, resulting in 4 points per side, plus an additional point in the centre of mass of the cube. Using this approach, together with the point coupling stated in Eq. (3), the coupling points form an extended body that can theoretically be made to resemble any arbitrary shape, in our case a cube. It is not trivial to accurately model cubic colloids and any approach requires a separate check in order to verify our model. We conducted simulations in periodic bound-

Table 1

Simulation parameters in simulation units (SU) and corresponding SI values. The unit for energy is defined by E_{kin}^{cube} , the kinetic energy of cube at $100\mu\text{m s}^{-1}$.

Quantity	Value (SI)	SU
Length unit	$2 \times 10^{-6} \text{m}$	1
Mass unit	$8 \times 10^{-15} \text{kg}$	1
Energy unit	$10^4 E_{kin}^{cube} (100\mu\text{m s}^{-1})$	1
Time unit	$6.8 \times 10^{-5} \text{s}$	1
Cube side length	$5 \times 10^{-6} \text{m}$	2.5
Density silica	2650kg m^{-3}	2.65
Cube Mass	$1.4 \times 10^{-13} \text{kg}$	17.2
Cube Rot. Inertia	$9.5 \times 10^{-25} \text{kg m}^2$	28.8
Solvent kin. viscosity	$8.9 \times 10^{-8} \text{m}^2 \text{s}^{-1}$	1.52
Solvent density	10^3kg m^{-3}	1

any conditions to extract the friction coefficients of a single colloid in a thermalised fluid at 298 K. Since the diffusion of the colloid is determined by the hydrodynamic interaction with the carrier, we can verify that the raspberry representation in simulations reflect a real system. The translational friction has been extracted by measuring the mean-square-displacement. The rotational friction coefficient has been extracted by measuring the decorrelation time of the orientation of the cube. For a chosen LB friction $\gamma_{LB} = 23$, the computation resulted in a translational friction coefficient $\gamma_{sim}^T = 6.002 \times 10^{-8} kg s^{-1}$. This value is roughly 3.4% larger than the coefficient calculated through Eq. (1), $\gamma_{theory}^T = 5.805 \times 10^{-8} kg s^{-1}$. The simulated value for the rotational friction, $\gamma_{sim}^R = 9.035 \times 10^{-19} kgm^2 s^{-1}$, is 1.3% larger than the calculated one from Eq. (2), $\gamma_{theory}^R = 8.919 \times 10^{-19} kgm^2 s^{-1}$. Since both of these equations assume a perfect cube (shape parameter $q = \infty$), we are satisfied with the return values of the simulations since superballs with a lower q than infinity experience a lower friction than a perfect cube [23].

The activity of the colloid is modelled by a force/counter-force formalism that applies a constant force on the centre of mass of the colloid and a counter-force of the same magnitude to the fluid at some distance l_f away from the colloid. Due to the counter-force, the system is momentum free. This approach, together with the raspberry model for an extended object, creates a complex hydrodynamic flow field which can be checked for the presence of higher hydrodynamic moments which were previously used to explain the oscillatory motion in channels for rods and cylinders. This can be done by a Legendre Fourier decomposition procedure,

$$\vec{u} = \kappa \vec{u}_D + \nu \vec{u}_Q + \mu \vec{u}_{SD} + o_1 \vec{u}_{o_1} + o_2 \vec{u}_{o_2} + \dots \quad (5)$$

Here, \vec{u}_D is the Stokes dipole, \vec{u}_Q the quadrupole, \vec{u}_{SD} the source dipole term, \vec{u}_{o_1} and \vec{u}_{o_2} the octupole and source octupole moment terms. The procedure for the decomposition in cylindrical coordinates is,

$$u_{x,n}(r) = \frac{2n+1}{2} \int_0^\pi \sin(\theta) L_n(\cos(\theta)) u_x(r, \theta) d\theta \quad (6)$$

which calculates $u_{x,n}(r)$ for either component $x = r, \theta$ and mode index n . A series of power law decays can be fitted to obtain the coefficients in Eq. (5). The decays for the r component and their corresponding fits are shown in Fig. 1. For a detailed explanation of the

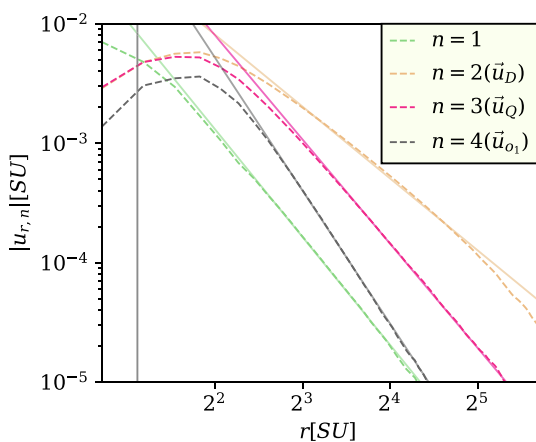


Fig. 1. Decay of the hydrodynamic moments from the Fourier Legendre decomposition procedure used in Reference [38], calculated for a single active cube in a box with periodic boundary conditions. Dashed lines correspond to simulation data for each moment encoded by colours. Solid lines are fits, from which the coefficients of the decomposition are extracted. The vertical Gray line marks $r = 2.5\sqrt{3}/2\sigma$ (half the diagonal of the cube), the hydrodynamic extend of the cubic colloid.

decomposition procedure, we refer to reference [38]. The extracted coefficients from the fits are: $\kappa = 0.065, \nu = 0.19, \mu = 0., o_1 = 0.31, o_2 = 0$. As expected from the force/counter-force formalism raspberry, there is no source dipole or source octupole moment detected. The other values are in line with the values obtained for cylinders and rods, κ and ν being close to the coefficients of a cylinder and o_1 being close to that of a rod. It is important to mention that for $n = 3$ and $n = 4$, we obtain a slower decay compared to the reported decay of r^{-3} and r^{-4} , respectively. For our fits, the best fitting results for those two moments were found to be in the order $r^{-2.8}$ and $r^{-3.7}$, which hints at a slightly lower decay of those moments.

Having fully characterised the raspberry model for our cube, we now turn to its behaviour in a micro channel. The simulation domain consists of two planar walls separated by a distance H along the x-axis of the channel, enclosing a non-thermalised LB fluid with the properties provided in Table 1. This set-up allows us to investigate the influence of only the hydrodynamic flow field, induced by activity, on the reorientation of our cubes, letting us draw direct comparisons to research done on rods, cylinders and spheres that do not take Brownian forces into account. The orientation of the colloids will hence be determined by the interaction of the colloid with the active flow field in the channel, the lateral motion by the active force and the friction of the fluid. The domain has periodic boundaries along the y- and z-axes. Simulation time for all shown results is 7s. The direction of the active force, hence the active velocity \vec{v}_a , is oriented to coincide with the [111] diagonal of the cube body (see Fig. 2). The magnitude of the applied active force, f_a leads to a swimming velocity of $100\mu m s^{-1}$ [39,40] in a simulation box with no walls and periodic boundary conditions. The counter-force is applied to the fluid 1.5 LB lattice sizes away from the closest coupling point of the cube, to ensure that the swimming velocity in simulations is not more than 3% smaller than the predicted swimming velocity $|\vec{v}_a|_{theory} = f_a/\gamma_{cube}^T$. Initially, the colloids centre of mass is placed exactly at the centre of the channel, or at a relative offset $r.o. = (H/2) + H\Delta x_0$ along the x-axis, with the active force and the channel walls enclosing a "starting angle" ϕ_0 , the latter being measured in the mathematical positive sense around the y-axis, with $\phi_0 = 0$ representing alignment with the z-axis. The colloids velocity vector is set to 0 before the start of the simulation, after that the colloid is free to move along and rotate around all axes. We additionally define a Weeks-Chandler-Andersen potential with $\epsilon = 1$ between each coupling point of the cube and the boundaries of the channel, repeling the cube for distances $r < \sqrt[3]{2}\sigma$, preventing the cube from moving through the wall,

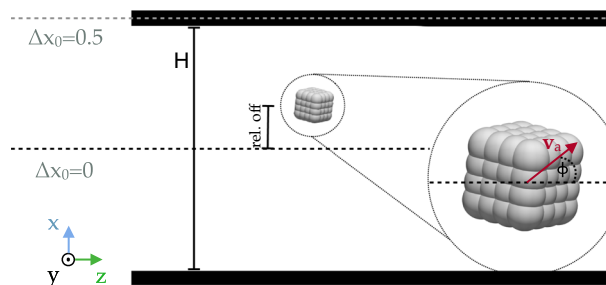


Fig. 2. Schematic representation of the simulation set up for a cube in a micro channel of height H . The active velocity vector \vec{v}_a stands in angle ϕ with the planar channel walls (shown in zoom-in). The relative offset of the starting position of the cube in simulations is displayed in terms of Δx_0 , with the offset being $r.o. = (H/2) + H\Delta x_0$.

$$u_{WCA} = 4\epsilon \left[\left(\frac{\sigma}{r} \right)^{12} - \left(\frac{\sigma}{r} \right)^6 \right] + \epsilon \text{ if } r < \sqrt[6]{2}\sigma; \quad 0 \text{ else.} \quad (7)$$

The dependence of the trajectories on the above choices is part of the further analysis of this article.

3. Trajectory analysis

We first analyse the trajectories by plotting the position of the centre of mass of a pusher cube in the x - z -plane of a channel with a wall separation of $H = 40\mu\text{m}$. The result is shown in Fig. 3, for an offset of $\Delta x_0 = 0$, meaning that at time zero the cube is positioned in the centre of the channel, plus for a range of starting angles ϕ_0 . The curves shown were selected to graphically represent the behaviour of the colloid best. In the figure, we can see that the cube is following a stable trajectory parallel to the channel walls for ϕ_0 between 0 and 20 degrees. This stands in stark contrast to the motion of a pusher rod or cylinder, that display an oscillatory motion around the channel centre axis with an increasing amplitude. Interestingly, the cube does not prefer a trajectory along this centre axis neither, but can find a stable trajectory at a certain distance from the wall depending on the initial starting angle ϕ_0 . Before entering those parallel to the wall trajectories, there are oscillations which are especially well seen for $\phi_0 = 0^\circ, 5^\circ, 10^\circ, 20^\circ$. We attribute this effect to the initial orientation of the cube around its active velocity vector (see Fig. 2). Since we do not take special care of this initial orientation, but only orient the velocity vector so it stands in an angle ϕ_0 with the walls, there is an additional rotational degree of freedom introduced by the anisotropic shape of the cube that is the orientation around the vector itself. This manifests itself during the first two oscillations, where we see a reorientation of the cube along the velocity vector before settling for a fixed orientation, indicating that once it has, the oscillations are dampened until the trajectory becomes linear.

For ϕ_0 larger than 20° , the cube is moving steadily towards the wall before touching and sliding along it. At this point, we have to make a technical remark. The used implementation of Lattice Boltzmann does not consider lubrication effects at walls, as well as proper near field effects close to the body of the cube due to poorer resolution, that might play an important role of reorientation near the wall. Researchers have an ongoing discussion about the weight with which near field hydrodynamic effects do affect the reorientation at boundaries. We therefore emphasise that the results for when the closest coupling point of the cube is getting closer than approximately 3 LB lattice lengths are missing those near field effects in a high resolution. This statement is primarily based on the flow field analysis done in the Methods section, shown in Fig. 1, where it is seen that the flow field starts to decay to the expected far field solution around 3 LB sites away from the

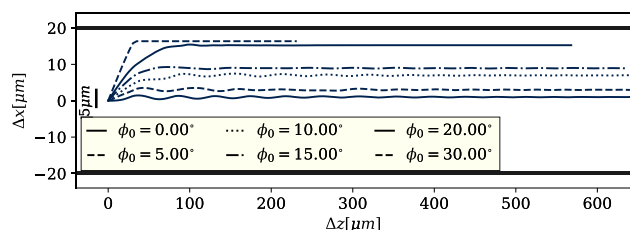


Fig. 3. Trajectories of the centre of mass of a single pusher cube with an active velocity of $100\mu\text{m s}^{-1}$ in the x - z -plane of a $40\mu\text{m}$ wide channel, for an initial spatial offset $\Delta x = 0$ and a range of initial angles ϕ_0 distinguished by line styles as shown in the legend. The $5\mu\text{m}$ scalebar at the left hand side of the plot shows the side length of the cube. The two horizontal black bars at -20 and $20\mu\text{m}$ mark the walls enclosing the fluid. 0 on the y -axis marks the centre of the channel in x -direction, 0 on the x -axis the starting point of the cube in z -direction.

closest coupling point making the cubic shape. In our simulations, any trajectory that includes the event of a coupling point getting closer than that, resulted in the cube sliding along the wall with the active force steadily pushing the cube towards the wall. Hence, we consider any of those trajectories in further analysis as sliding along the wall. Further investigation of this subject is of high interest, experimentally and numerically, as the large area of attack that the face of a cube poses will greatly vary the dynamics of the colloids close to a boundary, expectedly promoting a more steady sliding along walls than, for example, spheres exhibit. Although we have pointed out hydrodynamic similarities between cubes and spheres, the observed behaviour of cubes differ substantially from that of spheres. A spherical particle will be hydrodynamically attracted to a flat surface and any occurring oscillations in its trajectory are usually contributed to the competition between hydrodynamic and repulsive forces between surface and colloid, meaning that the particle only experiences small oscillations if it finds itself closer than its body length to the wall [20]. Neither for rods, cylinders nor cubes this is the case, as the oscillations occur even far away from the wall where the repulsive forces from the wall are zero. Inspecting the flow field of the cube in detail, we can find an explanation for the colloid stabilising along a parallel trajectory to the wall opposed to the continuous oscillation of a rod. Fig. 4 shows an exemplary state of the cube, $7\mu\text{m}$ away from the wall and at an angle $\phi \approx 11^\circ$, after finding its steady orientation around its velocity vector, but still performing a lateral oscillatory motion. The figure shows an asymmetry in the flow field around the axis perpendicular to the wall and through the cube centre of mass, causing a pressure difference between the cube faces that are closer to the walls compared to the ones that are further away. This results in the cube being rotated away from the wall for cases where the active velocity is enclosing a positive angle with the walls and in reverse, being rotated towards the wall in case the angle is negative. The rotation is visualised in the zoom-in of the cube in Fig. 4, showing the velocity of each coupling point of the

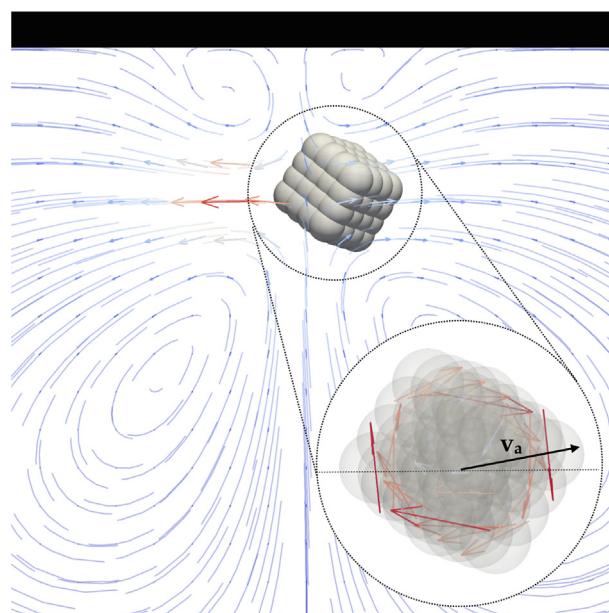


Fig. 4. Visualisation of the flow field around the cube in the laboratory frame. The flow lines are supported by arrows showing the direction of the flow and are scaled and coloured by fluid velocity magnitude. The zoom-in shows the cube in the same state of the simulation, with the arrows depicting the velocity of each coupling point in the cube centre of mass frame. The colour and opacity of the arrows in the zoom-in are scaled by coupling point velocity magnitude, independently of the fluid scaling.

cube in the cube centre of mass frame. This also explains the fact that the cubes can follow a trajectory that is not in the centre of the channel, but essentially any line that is parallel to the walls, since any deviation from $\phi = 0$ induces a torque on the cube bringing it into a stable trajectory, regardless of its distance from the wall. Although we did not perform simulations that only include a single wall rather than a channel, we expect the behaviour along a single wall to be similar, since the flow field dominating this dynamics is the one reflected from the wall that is closest to the cube.

3.1. Influence of the channel width

Knowing the above results, it seems natural to check the impact of the channel width, as a cube could potentially have more time to relax towards a steady trajectory in a wider channel before hitting the boundary. We repeat the above experiments, but set the channel width to $H = 56\mu\text{m}$. The particle is again placed at a relative offset from the centre of the channel as is also mentioned in the Methods section: $r.o. = (H/2) + H\Delta x_0$, where Δx_0 is chosen between 0 and 0.3. Note that the same value for Δx_0 leads to a different initial separation from the closest wall, hence a larger room for the colloid to relax its trajectory, for the two channel widths. For example, $\Delta x_0 = 0.2$ means that, at the beginning of the simulation, the cube is $16\mu\text{m}$ away from the closest wall for $H = 40\mu\text{m}$ and $22.4\mu\text{m}$ away for $H = 56\mu\text{m}$. For both values for H , we define two events: **A**: The colloid finds a stable trajectory parallel to the wall and never comes closer than 3 LB lattice lengths to the wall. **B**: The colloid touches the wall and slides along it. A stability map of the two outcomes for a range of Δx_0 and ϕ_0 is seen in Fig. 5. Fig. 5 shows that a wider channel gives more headroom for the cube to relax towards a steady trajectory and therefore a wider range of the initial conditions lead to a steady trajectory. Since the active velocity in both cases is $100\mu\text{m s}^{-1}$ (note that this is the active eigen velocity and not the effective velocity typically obtained from measuring diffusion in experiments), we repeated

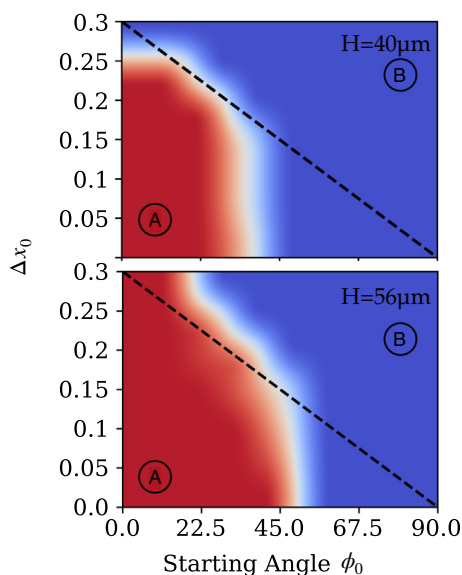


Fig. 5. Stability map showing the condition of initial displacement Δx_0 and ϕ_0 of the colloid from the centre of the channel for two outcomes: **A**: The colloid finds a stable trajectory parallel and never comes closer than 3 LB lattice lengths to the wall. **B**: The colloid touches the wall and slides along it. The region for outcome **A** is coloured in red, the region for **B** is blue; both are marked by the corresponding circled letter. The upper plot is for a wall separation of $H = 40\mu\text{m}$, the lower for $H = 56\mu\text{m}$. The phase map colours are interpolated between results for 20 values of each, Δx_0 and ϕ_0 .

the simulations for both channel widths and $|\vec{v}_a| = 50, 25\mu\text{m s}^{-1}$ to see if it affects the results. Interestingly, we could not detect a difference in trajectories for different active velocities. It would first be intuitive to think that the faster particle would be more likely to hit the wall at steeper ϕ_0 , but since the force that is pushing the cube is always directly applied back to the fluid, the flow field that is causing the reorientation of the cube is proportionally increasing as well, leading to the same behaviour.

3.2. Influence of the active dipole separation

One parameter given to simulations is the dipole length l_f , the distance between the points where the active force is applied to the particle and the counter-force is applied to the fluid, which, together with the force magnitude, determines the dipole strength and therefore the swimming velocity of the colloid. We are bound by numerical considerations to a separation that applies the counter-force outside the body of the cube, at least one LB lattice length away from the closest coupling point, to reach swimming velocities that are within 10% of the predicted swimming speed $|\vec{v}_a| = f_a / \gamma_{cube}^T$, where f_a is the magnitude of the active force and γ_{cube}^T is the friction from Eq. (1). This introduces an asymmetry of the flow field with respect to an axis going through the cubes centre, as is visible in Fig. 4. Since we attribute the reorientation of the cube to the pressure asymmetry on the sides of the cube, we need to check the influence of the dipole length on the cube trajectories. The above experiments in a channel of height $H = 40\mu\text{m}$ were repeated for dipole lengths so that the force is not applied 1.5 LB lattice lengths, but 2 and 3 lengths away from the closest coupling points. We see that the dipole length does not qualitatively influence the aforementioned findings; the colloids find a stable trajectory parallel to the wall for the same Δx_0 and ϕ_0 for every force/counter-force separation. However, the separation dampens the oscillation quicker for all initial conditions, further proving that the interaction with the asymmetric flow vortices is responsible for the behaviour of the oscillatory motion observed in the trajectories. In experiments, the type of propulsion mechanism will determine the exact form of the flow field and hence the detailed dynamics will be determined by rather detailed features as is demonstrated here. The detailed investigation of cubes with different propulsion mechanisms is therefore encouraged.

3.3. Influence of the active force orientation

All of the above results were obtained assuming that the active force is perfectly aligned with the diagonal of the cube. Of course, this assumption does not have to hold true for a potential cube used in an experiment, given that the active force from any propulsion mechanism can be easily misaligned with the diagonal. Hence, we below investigate how the trajectories change due to a misalignment with the [111] axis of the cubes body. Two more scenarios are taken into account. First, we keep the active force applied at the centre of mass of the cube, but let the force vector enclose a 5° angle with the diagonal axis, which is measured around the y-axis after initial placement of the cube in the simulation box. Second, additionally to setting the force at an angle, we apply it $1\mu\text{m}$ away from the centre of mass. Both scenarios were investigated in a channel with width $H = 56\mu\text{m}$, similar to the channel in Section 3.1. The trajectories for the first scenario are displayed in Fig. 6, for the second in Fig. 7. Shifting the active force by 5° does not lead to any qualitative changes in the behaviour; cubes will relax towards a linear trajectory parallel to the walls for a set of Δx_0 and ϕ_0 . Quantitatively, we see that the rate at which this happens (solid lines in Fig. 6)) to be lower than that for the case of a perfect alignment between active force and body diagonal

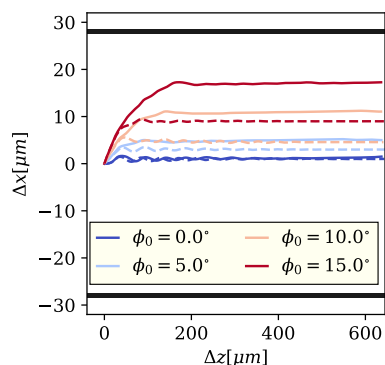


Fig. 6. Trajectories of two different cube species for $\Delta x_0 = 0$, distinguished by linestyle. **Dashed:** The active force is parallel to the [111] axis of the cubes body; **Solid:** The active force encloses a 5° angle with the [111] axis of the cubes body. The curves are coloured by starting angle ϕ_0 ; black bars at the top and bottom denote the walls that enclose the channel of width $H = 56\mu\text{m}$.

(dashed lines in Fig. 6). The shown trajectories are for $\Delta x_0 = 0$ and ϕ_0 up to the last investigated value before the cube touches the wall. The parallel case shows a significantly faster relaxation towards the final linear trajectory than its non-parallel counterpart. The oscillatory motion experienced for the aligned case, at any ϕ_0 , is not visibly detected for any trajectory of the non-aligned case except for $\Delta x_0 = 0$, due to the change in orientational relaxation around the active force vector that is also responsible for the occurrence of the oscillations discussed in Fig. 3. In case of a non aligned propulsion force, with respect to the body diagonal as well as the centre of mass, the trajectories show a significant deviation from the rest of the configurations tested in the previous experiments, reminiscent of active chiral or tumbling motion [39,41–43](Fig. 7). For $\Delta x_0 = 0$, the cubes lateral positions for all

axes rotate around the centre of the channel during the 7 s simulation time. This is seen in Fig. 7, showing the motion of the cube in x- and z-direction as in previous results, but also encoding motion along the y-axis of the channel with colours. If, however, the initial position of the cube is close enough to the wall so that the anisotropy of the flow field and the hydrodynamic interactions between a wall and a cube start to come into play, the cube experiences a slow drift towards the wall, decreasing their distance with every rotation in the trajectory.

Another obvious orientation of the active force would be along the [100] axis of the cube body, so pointing out of the side of the cube. For the whole investigated range of Δx_0 and ϕ_0 , every cube was immediately drifting to the wall with no oscillations or reorientation process happening. Here, we see the peculiarities of the cube as a hydrodynamic shape come into play. Although it behaves like a sphere in a steady flow with an independence of rotational and lateral motion, the active force, hence the flow field, in relation the cube orientation greatly diversifies the behaviour and trajectories of the cubes. The reorientation process explained with Fig. 4 does not work anymore for the case of a [100] orientation of the active force and a experimentally synthesised active colloid will show a greatly varying behaviour depending on the realisation of the propulsion mechanism.

3.4. Cylindrical boundary – Tube

Having shown the trajectories of active micro cubes between two planar walls, we now turn to a cylindrical constraint to show that a change to a different boundary symmetry preserves the behaviour. The procedure is similar to the previous experiments in the first part of this section, simply exchanging the planar walls with a cylinder with a diameter of $40\mu\text{m}$. This eliminates the periodic boundary conditions along the y-axis, as was the case for the

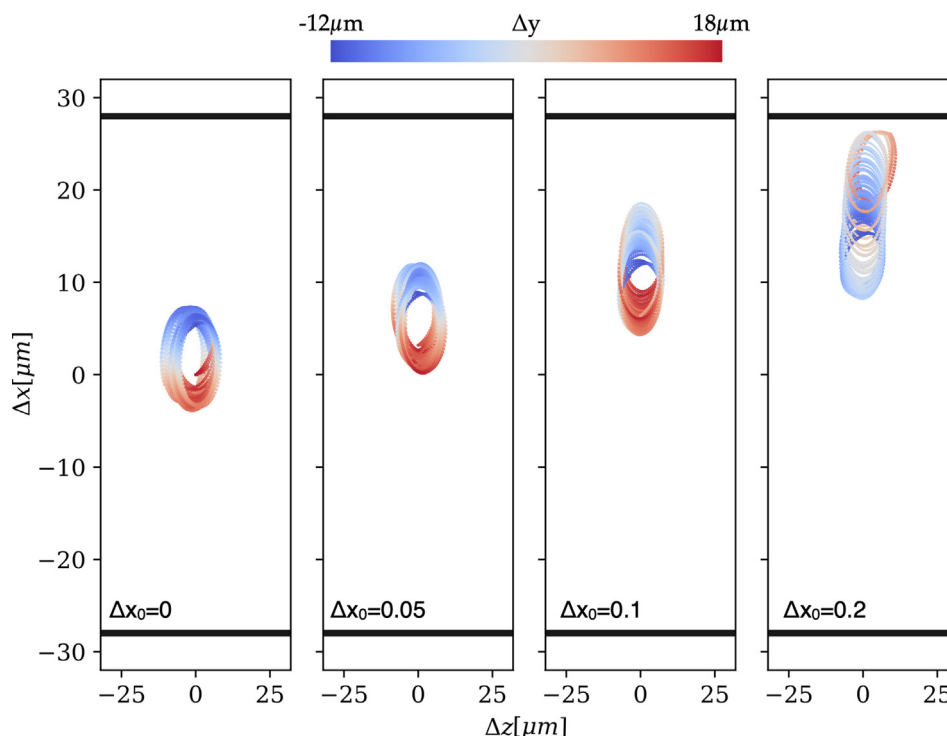


Fig. 7. Series of tumbling trajectories of a cube with active force that is applied $1\mu\text{m}$ away from the cubes centre of mass and at an angle of 5° with the cubes [111] diagonal. The starting position Δx_0 is increased from the left to the right panel and is marked in the bottom left corner of each panel. Black bars at the top and bottom denote the walls that enclose the channel of width $H = 56\mu\text{m}$. The colouring of the trajectories show the displacement in the y-direction of the channel, as marked in the colour bar at the top. The alternating colours of the leftmost panel indicate an oscillation in y-direction of the channel, similarly to the oscillation in x- and z-direction.

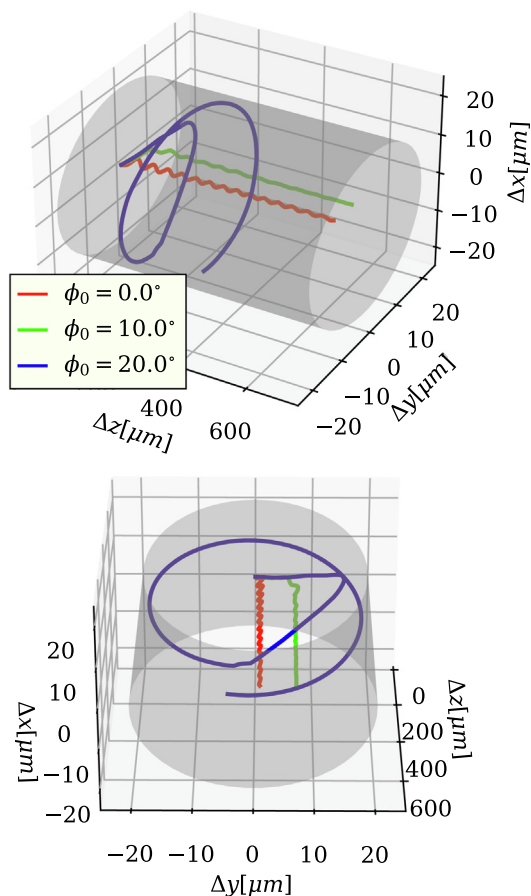


Fig. 8. Trajectories of cubes in a tube with diameter $40\mu\text{m}$, outlined as a Gray cylinder, for three starting angles ϕ_0 distinguished by colour; red: 0° ; green: 10° ; blue: 20° . The upper and lower plot show the same result from different angles.

walls, and makes the boundary fully radially symmetric around the cylinder axis. Fig. 8 shows a selection of trajectories that best represent the system while maintaining readability of the plot. In line with the results presented above, cubes that have an initial angle ϕ_0 smaller than 20° , first experience a force that tries to push them closer to the sides of the channel, which leads to the same oscillatory motion around an axis that is parallel to the cylinder axis. After the flow field fully developed, the cubes eventually reach a stable trajectory off channel centre. The angle of oscillation with respect to the cylinder axis is now fully determined by the initial orientation of the cube around its velocity vector due to the radial symmetry of the boundary, opposed to the case of planar boundaries where the cube is reoriented inside the channel. This oscillation only happens in one plane and is not helical like for rods. For ϕ_0 larger than 20° , cubes are hitting the cylinder side and slide along it. However, the nature of this helical motion, e.g. the orientation of the rotation along the tube walls, depends on the near-field interaction of the cube with the boundary and appropriate corrections would need to be made in order to obtain a precise picture.

4. Conclusion

In this article, we have analysed trajectories of active cubes in micro channels to highlight their distinct hydrodynamic behaviour and differences to spheres, rods and cylinders, previously investigated in a similar setting. We have found that compared to other shapes, active cubes in micro channels do neither experience the

commonly observed attraction to planar walls, nor the same oscillatory behaviour around the channel centre that pusher and puller rods exhibit. Instead, for a cube that has its active velocity vector aligned with its body diagonal, a set of initial conditions that is constituted by the distance to the wall and the angle of the active force vector relative to the wall, determines whether the cube moves near the centre of the channel parallel to the wall or comes into its close proximity. Only few oscillations are observed before the cube relaxes to its final steady trajectory. We find this to be true for a range of factors that we accounted for in simulations: active velocity, channel width and the separation of active force/counter-force application points. One factor which exploits the geometry of the cube which has major implications for the trajectories, is the alignment of the active force within the body of the cube. If the active force stands at an angle to the body diagonal, the initial oscillations are damped and the cube relaxes at a different rate to its final trajectory. If in addition, the active force is not applied at the centre of mass but at a slightly shifted position, the cube performs helical motion either around the centre of the channel, or helical motion with a slow drift towards the closest wall, depending on the initial condition. All of the above results are attributed to the unique hydrodynamic behaviour of a cube which is like that of a sphere in laminar Stokes flow, but becomes more complicated in the presence of a complex flow field as is the one produced by an active colloid. Our findings promote the closer investigation of active cubic colloids, considering that the hydrodynamic interaction between them and boundaries are not yet understood in detail, despite having the potential to show substantially different behaviour and might therefore be used in different applications than synthetic spheres or rods.

Declaration of Competing Interest

The authors declare that they have no known competing financial interests or personal relationships that could have appeared to influence the work reported in this paper.

Acknowledgements

The research was supported by FWF Project SAM P 33748 and Russian Science Foundation Grant No.19-12-00209. Computer simulations were performed at the Vienna Scientific Cluster (VSC).

References

- [1] J.R. Howse, R.A. Jones, A.J. Ryan, T. Gough, R. Vafabakhsh, R. Golestanian, Self-motile colloidal particles: from directed propulsion to random walk, *Phys. Rev. Lett.* 99 (4) (2007) 048102.
- [2] S.J. Ebbens, J.R. Howse, In pursuit of propulsion at the nanoscale, *Soft Matter* 6 (4) (2010) 726–738.
- [3] H. Ke, S. Ye, R.L. Carroll, K. Showalter, Motion analysis of self-propelled Pt-silica particles in hydrogen peroxide solutions, *The Journal of Physical Chemistry A* 114 (17) (2010) 5462–5467.
- [4] S.E. Spagnolie, E. Lauga, Hydrodynamics of self-propulsion near a boundary: predictions and accuracy of far-field approximations, *J. Fluid Mech.* 700 (2012) 105–147.
- [5] L. Caprini, F. Cecconi, C. Maggi, U. Marini Bettolo Marconi, Activity-controlled clogging and unclogging of microchannels, *Phys. Rev. Research* 2 (2020) 043359, <https://doi.org/10.1103/PhysRevResearch.2.043359>.
- [6] U. Marini Bettolo Marconi, A. Sarracino, C. Maggi, A. Puglisi, Self-propulsion against a moving membrane: Enhanced accumulation and drag force, *Phys. Rev. E* 96 (2017) 032601, <https://doi.org/10.1103/PhysRevE.96.032601>.
- [7] Z. Shen, A. Würger, J.S. Lintuvuori, Hydrodynamic interaction of a self-propelling particle with a wall, *The European Physical Journal E* 41 (3) (2018) 1–9.
- [8] M. Kuron, P. Stärk, C. Holm, J. De Graaf, Hydrodynamic mobility reversal of squirmers near flat and curved surfaces, *Soft Matter* 15 (29) (2019) 5908–5920.
- [9] S. Das, A. Cacciuto, Colloidal swimmers near curved and structured walls, *Soft Matter* 15 (41) (2019) 8290–8301.
- [10] G. Li, J.X. Tang, Accumulation of microswimmers near a surface mediated by collision and rotational Brownian motion, *Phys. Rev. Lett.* 103 (7) (2009) 078101.

- [11] J. Elgeti, G. Gompper, Wall accumulation of self-propelled spheres, *Europhys. Lett.* 101 (4) (2013) 48003.
- [12] H. Wensink, H. Löwen, Aggregation of self-propelled colloidal rods near confining walls, *Phys. Rev. E* 78 (3) (2008) 031409.
- [13] J. Elgeti, G. Gompper, Self-propelled rods near surfaces, *Europhys. Lett.* 85 (3) (2009) 38002.
- [14] A. Zöttl, H. Stark, Emergent behavior in active colloids, *J. Phys.: Condens. Matter* 28 (25) (2016) 253001.
- [15] G.-J. Li, A.M. Ardekani, Hydrodynamic interaction of microswimmers near a wall, *Phys. Rev. E* 90 (1) (2014) 013010.
- [16] K. Schaar, A. Zöttl, H. Stark, Detention times of microswimmers close to surfaces: Influence of hydrodynamic interactions and noise, *Phys. Rev. Lett.* 115 (3) (2015) 038101.
- [17] W. Uspal, M.N. Popescu, S. Dietrich, M. Tasinkevych, Rheotaxis of spherical active particles near a planar wall, *Soft Matter* 11 (33) (2015) 6613–6632.
- [18] A.P. Berke, L. Turner, H.C. Berg, E. Lauga, Hydrodynamic attraction of swimming microorganisms by surfaces, *Phys. Rev. Lett.* 101 (3) (2008) 038102.
- [19] S. Wang, A. Ardekani, Swimming of a model ciliate near an air-liquid interface, *Phys. Rev. E* 87 (6) (2013) 063010.
- [20] J.S. Lintuvuori, A.T. Brown, K. Stratford, D. Marenduzzo, Hydrodynamic oscillations and variable swimming speed in squirmers close to repulsive walls, *Soft Matter* 12 (38) (2016) 7959–7968.
- [21] J. de Graaf, A.J. Mathijssen, M. Fabritius, H. Menke, C. Holm, T.N. Shendruk, Understanding the onset of oscillatory swimming in microchannels, *Soft Matter* 12 (21) (2016) 4704–4708.
- [22] H. Masoud, B.I. Bingham, A. Alexeev, Designing maneuverable microswimmers actuated by responsive gel, *Soft Matter* 8 (34) (2012) 8944–8951.
- [23] S. Ouhajji, Chiral and Active Colloids, Ph.D. thesis, University Utrecht, 2019.
- [24] O. Petrichenko, G. Kitenbergs, M. Brics, E. Dubois, R. Perzynski, A. Cēbers, Swarming of micron-sized hematite cubes in a rotating magnetic field—Experiments, *J. Magn. Magn. Mater.* 500 (2020) 166404.
- [25] J. Donaldson, E. Pyanzina, E. Novak, S. Kantorovich, Anisometric and anisotropic magnetic colloids: How to tune the response, *J. Magn. Magn. Mater.* 383 (2015) 267–271, <https://doi.org/10.1016/j.jmmm.2014.11.013>.
- [26] J.G. Donaldson, E.S. Pyanzina, S.S. Kantorovich, Nanoparticle Shape Influences the Magnetic Response of Ferro-Colloids, *ACS Nano* 11 (8) (2017) 8153–8166, <https://doi.org/10.1021/acsnano.7b03064>.
- [27] S. Schyck, J.-M. Meijer, L. Baldauf, P. Schall, A.V. Petukhov, L. Rossi, Self-assembly of colloidal superballs under spherical confinement of a drying droplet, *Journal of Colloid and Interface Science Open* 5 (2022) 100037, <https://doi.org/10.1016/j.jciso.2021.100037>, ISSN 2666-934X.
- [28] M. Kaiser, Y. Martinez, A.M. Schmidt, P.A. Sánchez, S.S. Kantorovich, Diffusion of single active-dipolar cubes in applied fields, *J. Mol. Liq.* 304 (2020) 112688.
- [29] M. Kaiser, S.S. Kantorovich, Flux and separation of magneto-active superballs in applied fields, *PCCP* 23 (41) (2021) 23827–23835.
- [30] K. Okada, A. Satoh, Evaluation of the translational and rotational diffusion coefficients of a cubic particle (for the application to Brownian dynamics simulations), *Mol. Phys.* 118 (5) (2020) 1631498.
- [31] J.K. Dhont, W.J. Briels, Rod-like Brownian particles in shear flow, *Soft Matter: Complex Colloidal Suspensions*, edited by G. Gompper, M. Schick 2.
- [32] M. Doi, S.F. Edwards, S.F. Edwards, *The theory of polymer dynamics*, vol. 73, Oxford University Press, 1988.
- [33] F. Weik, R. Weeber, K. Szuttor, K. Breitsprecher, J. de Graaf, M. Kuron, J. Landsgesell, H. Menke, D. Sean, C. Holm, ESPResSo 4.0—an extensible software package for simulating soft matter systems, *The European Physical Journal Special Topics* 227 (14) (2019) 1789–1816.
- [34] D. Röhm, A. Arnold, Lattice boltzmann simulations on gpus with espresso, *The European Physical Journal Special Topics* 210 (1) (2012) 89–100.
- [35] P. Ahlrichs, B. Dünweg, Simulation of a single polymer chain in solution by combining lattice Boltzmann and molecular dynamics, *J. Chem. Phys.* 111 (17) (1999) 8225–8239.
- [36] L. Rossi, S. Sacanna, W.T. Irvine, P.M. Chaikin, D.J. Pine, A.P. Philipse, Cubic crystals from cubic colloids, *Soft Matter* 7 (9) (2011) 4139–4142.
- [37] J.-M. Meijer, F. Hagemans, L. Rossi, D.V. Byelov, S.I. Castillo, A. Snigirev, I. Snigireva, A.P. Philipse, A.V. Petukhov, Self-assembly of colloidal cubes via vertical deposition, *Langmuir* 28 (20) (2012) 7631–7638.
- [38] J. de Graaf, H. Menke, A.J. Mathijssen, M. Fabritius, C. Holm, T.N. Shendruk, Lattice-Boltzmann hydrodynamics of anisotropic active matter, *J. Chem. Phys.* 144 (13) (2016) 134106.
- [39] C. Bechinger, R. Di Leonardo, H. Löwen, C. Reichhardt, G. Volpe, G. Volpe, Active particles in complex and crowded environments, *Rev. Mod. Phys.* 88 (4) (2016) 045006.
- [40] X. Ma, K. Hahn, S. Sanchez, Catalytic mesoporous Janus nanomotors for active cargo delivery, *J. Am. Chem. Soc.* 137 (15) (2015) 4976–4979.
- [41] F. Kümmel, B. Ten Hagen, R. Wittkowski, I. Buttinoni, R. Eichhorn, G. Volpe, H. Löwen, C. Bechinger, Circular motion of asymmetric self-propelling particles, *Phys. Rev. Lett.* 110 (19) (2013) 198302.
- [42] E. Lauga, W.R. DiLuzio, G.M. Whitesides, H.A. Stone, Swimming in circles: motion of bacteria near solid boundaries, *Biophysical journal* 90 (2) (2006) 400–412.
- [43] T. Ohta, T. Ohkuma, Deformable self-propelled particles, *Phys. Rev. Lett.* 102 (15) (2009) 154101.